

Distance of W3(OH) by VLBI annual parallax measurement

K. Hachisuka¹, A. Brunthaler^{2,1}, Y. Hagiwara³, K. M. Menten¹, H. Imai⁴, M. Miyoshi⁵, and T. Sasao⁶

¹ Max-Planck-Institut für Radioastronomie, Auf dem Hügel 69, 53121 Bonn, Germany

² Joint Institute for VLBI in Europe, Postbus 2, 7990 AA Dwingeloo, The Netherlands

³ ASTRON, Westerbork Observatory, P.O. Box 2, 7990 AA Dwingeloo, The Netherlands

⁴ Department of Physics, Kagoshima University, Kagoshima 890-0065, Japan

⁵ National Astronomical Observatory, Mitaka, Tokyo 181-8588, Japan

⁶ Department of Space Survey and Information Technology, Ajou University, Suwon, 442-749, Republic of Korea

Abstract. The most powerful tool for measuring distances within our Galaxy is the annual parallax. We carried out phase-referencing VLBI observations of H₂O masers in the star forming region W3(OH) with respect to the extragalactic continuum source ICRF 0244+624 to measure their absolute proper motions. The measured annual parallax is 0.484 ± 0.004 milli-arcseconds which corresponds to a distance of $2.07^{+0.01}_{-0.02}$ kpc from the sun. This distance is consistent with photometric and kinematic distances from previous observations.

1. Introduction

The annual parallax is the most powerful tool for the determination of distances to objects in our Galaxy. The Hipparcos satellite successfully measured the distances to many stars in the Solar neighborhood. Those results contributed to various fields of modern astronomy (e.g. Perryman et al. 1995). However, annual parallax measurements for far-away sources with kpc distances using single telescopes are impossible, since the value of the annual parallax is very small, e.g., 1 milli arcsecond (mas) at a distance of 1 kiloparsecs (kpc). In fact, the Hipparcos satellite only determined the distances of stars within 200 pc from the Sun.

On the other hand, Very Long Baseline Interferometry (VLBI) provides the highest resolution in astronomy. In phase-referencing VLBI, the position of a target source is measured relative to a nearby positional reference source (see e.g. Beasley & Conway 1995 ; Ros 2003). The feasibility of annual parallax measurements with VLBI has been demonstrated by Brisken et al. (2002) who measured annual parallaxes of pulsars in the Galaxy and by van Langevelde et al. (2000) and Vlemmings et al. (2002) who measured distances of Galactic OH masers associated with late type stars. Their results indicate that VLBI astrometry can measure distances of up to a few kpc. Hence, a large part of the Milky Way can be accessed by VLBI. This enables us to understand the Galactic structure and dynamics by VLBI astrometry since many maser sources exist in the whole Galaxy (e.g. Wouterloot et al. 1993) and are high brightness VLBI targets.

As our first step into this field of study, we observed H₂O masers in the Galactic star forming region W3(OH) and, alternately, the close-by extragalactic continuum source J0244+624 with phase-referencing VLBI. Here we report the result of an annual parallax measurement of H₂O maser features in W3(OH).

2. Observation and data reduction

2.1. Observed sources

We selected W3(OH) as our target source since it is one of the strongest Galactic H₂O maser sources. Located in the Perseus arm, W3(OH) was thought to have a distance of about 2.3 kpc from the Sun (Georgelin & Georgelin 1976; Humphreys 1978). *Relative* proper motions of H₂O masers in W3(OH) have been measured before with VLBI (Alcolea et al. 1992). These masers move in a bipolar outflow, originating in the so-called Turner-Welch (TW) object, which is thought to be a high or intermediate-mass protostar (e.g., Reid et al. 1995; Wyrowski et al. 1999).

We used ICRF 0244+624 as a phase-reference source. Its angular separation from W3(OH) is 2.17 degrees. Since this source is extragalactic with a redshift of 0.0438 (Margon & Kwitter 1978), its own proper motion is negligible. It is also very strong and compact at lower frequencies (Fey & Charlot. 2000). Thus, it is very useful as a phase-reference source.

2.2. VLBA multi-epoch observations

Seven epochs of observations were made over the course of 16 months (Table 1). Time separations were from two to four months. Each observation was carried out during 4 hours including calibrator observations. NRAO150 was observed for 5 minutes every 44 minutes for delay and bandpass calibration. W3(OH) and ICRF 0244+624 were observed with fast antenna-switching phase-referencing mode and at high elevation. The typical elevation varied from 46 to 62 degrees. The switching cycle was 40 seconds at all epochs, typical on-source time was 7 seconds for W3(OH) and ICRF 0244+624, respectively.

All observations were made with the ten station NRAO VLBA¹. Two antennas (KP and LA) did not observe in the first epoch because of heavy snow, one antenna (PT) was flagged in the third and seventh epoch since most of the data was lost because of system troubles. Also, SC was flagged in all epochs, since it produced no useful data. All Data were recorded using the VLBA recorder with two base-band channels (BBCs) and a bandwidth of 16 MHz. Data correlation was made with 1024 spectral channels in each BBC with an integration time of 2 seconds. The resulting velocity spacing of each spectral channel was 0.224 km s^{-1} at 22.24 GHz.

Table 1. Summary of the VLBA observations.

	Epoch	Stations
2001/01/28	01:11:00 – 05:13:00 (UT)	7
2001/05/12	18:20:00 – 22:20:00 (UT)	9
2001/07/12	14:20:00 – 18:20:00 (UT)	8
2001/08/25	11:27:00 – 15:27:00 (UT)	9
2001/10/23	07:35:00 – 11:35:00 (UT)	9
2002/01/12	02:16:00 – 06:16:00 (UT)	9
2002/05/06	18:44:00 – 22:44:00 (UT)	7

2.3. Data reduction

The data were calibrated and imaged with standard techniques using the AIPS software package. A priori amplitude calibration was applied using system temperature measurements and standard gain curves. We calibrated clock offsets between antennas using the calibrator NRAO150. A fringe fit was performed on ICRF 0244+624 and the solutions were applied to W3(OH).

The largest errors in phase-referencing observations are introduced by a zenith delay error in the atmospheric model of the correlator. These errors will degrade the image quality and the astrometric accuracy. However, we modeled the calibrated phase data of the strongest maser feature as the result of an position offset and a zenith delay error at each station. These zenith delay errors can then be corrected by the AIPS task CLCOR. This correction improves the quality of the phase-referenced images and the astrometric accuracy (e.g. Brunthaler et al. 2003). The data of MK at the 7th epoch was flagged since we could not estimate the zenith delay error of this station.

After those corrections, we carried out fringe fitting for NRAO150 and ICRF 0244+624 again. Finally, we applied these revised solutions to the UV data of W3(OH) and created images of the maser features at each epoch.

To determine the position of each maser spot, we performed a two-dimensional Gaussian fit with the AIPS task JMFIT. We traced maser features between different epochs by taking account of their LSR velocities and posi-

tions. It is difficult to exactly trace the same maser feature since H_2O masers are highly time variable and their absolute proper motions relative to the extragalactic reference source were non-linear because of the effect of the parallax.

3. Results

3.1. Reference source: ICRF 0244+624

The extragalactic continuum source ICRF 0244+624 was detected in all epochs. The peak flux densities were always over 0.9 Jy/beam , which is strong enough for an excellent phase calibration. The structure of this source was compact and unresolved like in previous VLBI observations at lower frequencies. Positions of the peak between all epochs were fluctuating within $\pm 10 \mu\text{as}$ from the map origin. The standard deviations of the peak position were $6.5 \mu\text{as}$ in right ascension and $7.6 \mu\text{as}$ in declination, which we take as the uncertainty of the reference position.

3.2. Galactic H_2O maser source: W3(OH)

H_2O masers in W3(OH) were detected in all epochs. The peak flux densities were from a few hundred mJy to one thousand Jy. The masers were distributed over an area of $2.5'' \times 0.5''$ (Figure 1) which is consistent with previous VLBI observations (Alcolea et al. 1992). Figure 1 contains only the 15 maser features that were detected in at least 5 epochs. These features are listed in Table 2. The maser features were usually detected in 2 to 7 adjacent velocity channels. There were additionally many other short lived H_2O maser features.

The typical formal position error of each H_2O maser spot was $10 \mu\text{as}$ in right ascension and $20 \mu\text{as}$ in declination. Figure 2 shows the absolute proper motion of the maser feature 2 in Table 2. This proper motion is the sum of the inner motion in W3(OH), the annual parallax, the Galactic rotation, Solar motion and probably a peculiar motion of W3(OH) which might differ from the Galactic rotation. All motions except the annual parallax are linear motions. Also, these motions are equal for all maser features except the inner motion.

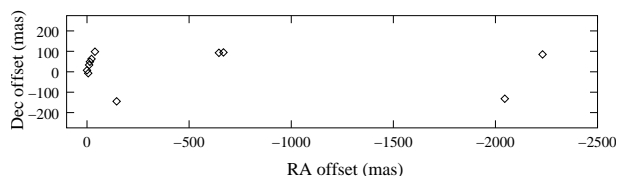


Fig. 1. Spatial distribution of H_2O maser features in W3(OH). The open square shows that the H_2O maser feature was detected over 5 epochs.

¹ The National Radio Astronomy Observatory is a facility of the National Science Foundation operated under cooperative agreement by Associated Universities, Inc.

Table 2. List of detected maser features. The columns give the name, number of channels with emission used in the model fit, number of epochs, position offset from the phase center at first detected epoch and LSR velocity.

No.	channels	epochs	Position offset		V_{LSR} (km s^{-1})
			$\Delta\alpha$ (mas)	$\Delta\delta$ (mas)	
1	4	7	-4.99	-5.6	-48.6
2	4	7	-9.68	33.4	-49.0
3	3	6	-7.72	33.3	-48.6
4	2	5	-5.62	32.9	-50.1
5	3	5	-13.70	49.2	-49.4
6	2	6	-21.68	63.2	-49.0
7	3	5	-19.54	62.2	-48.8
8	4	6	-38.16	97.9	-49.4
9	7	7	-144.50	-144.3	-51.1
10	4	5	-653.64	92.1	-52.6
11	2	6	-646.07	90.2	-51.5
12	4	5	-653.27	92.3	-51.9
13	3	6	-662.86	95.0	-54.7
14	5	7	-2045.84	-133.4	-45.2
15	5	6	-2231.28	84.1	-62.8

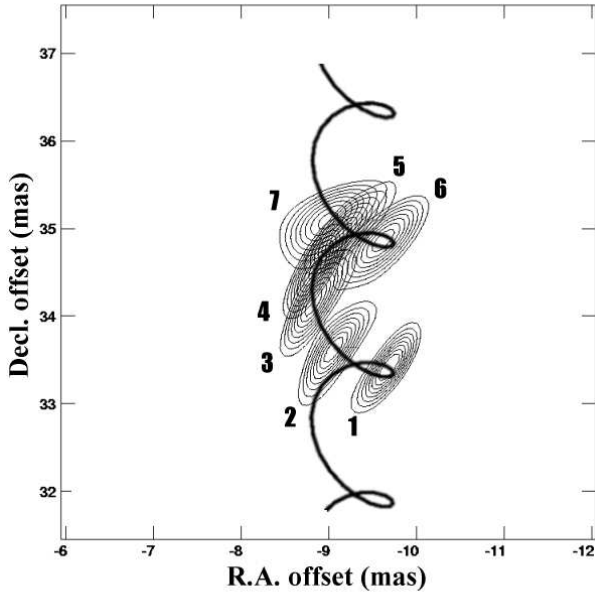


Fig. 2. Absolute proper motion of the H_2O maser feature at -49.0 km^{-1} (No. 2 in Table 2) in the image plane. The numbers indicate each epoch. Contours are 20, 30, 40, 50, 60, 70, 80, 90% of the peak of brightness. The peak flux density of 1st to 7th epoch was 430, 215, 204, 79, 31, 39, and 44 Jy/beam, respectively. Solid line shows the result of astrometric model fitting.

3.3. Annual parallax of maser features

We carried out a model fit of the path of the maser features in terms of its proper motion (μ_α, μ_δ) and annual parallax (Π) by

$$\Delta\alpha \cos \delta = \Pi f_\alpha(\alpha, \delta, t) + \mu_\alpha t + \alpha_0$$

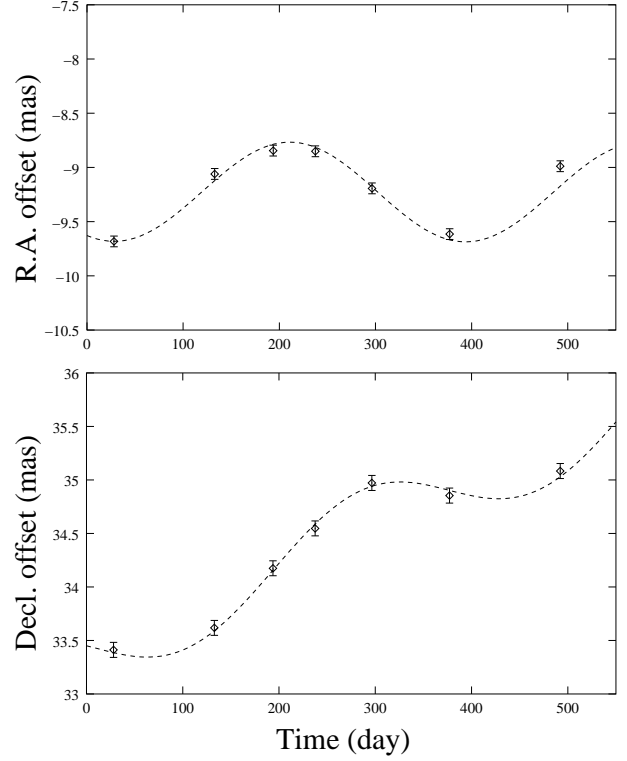


Fig. 3. Absolute proper motion of H_2O maser at LSR velocity of -49.0 km^{-1} (No. 2 in Table 2.) at right ascension and declination, respectively. The dashed line shows the best fit curve by the astrometric model fitting.

$$\Delta\delta = \Pi f_\delta(\alpha, \delta, t) + \mu_\delta t + \delta_0$$

where t is time. The functions f_α and f_δ are the parallax displacements in right ascension and declination, respectively. The origin of position for each maser feature, α_0 and δ_0 , is not discussed here.

Maser features 14 and 15 are located 2 arcseconds from the phase center and are affected by time-smearing effects. Hence, they were excluded from our analysis. We used a total of 45 different data sets (13 maser features in several velocity channels). We fit one annual parallax and 45 individual linear motions to the combined data set. We ignored any acceleration of maser features in the proper motions and radial velocities. The estimated annual parallax is $0.484 \pm 0.004 \text{ mas}$. Figure 3 shows the result of the astrometric model fitting for one channel of maser feature 2.

We also fitted a proper motion and an annual parallax to each of the 45 data sets individually. The errors of these individual parallaxes range from $\sim 0.01 \text{ mas}$ for strong components to $\sim 0.1 \text{ mas}$ for weak components. The parallaxes of the different maser features were in general consistent within the errors with the parallax from the combined fit. We can define a parameter R_i for each individual fit by

$$R_i = \frac{|\pi_i - \bar{\pi}|}{\Delta\pi_i},$$

where π_i and $\Delta\pi_i$ are the parallax and its error from fit i and $\bar{\pi}$ is the parallax from the combined fit.

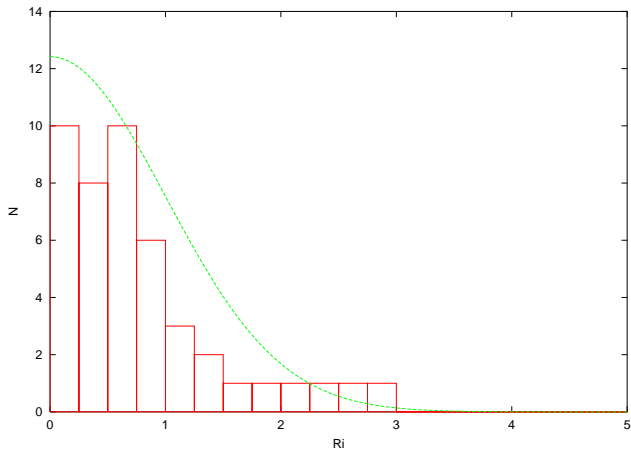


Fig. 4. Histogram of parameter R_i (see text) for the individual fits and the expectation from a Gaussian distribution of errors (dashed line).

A histogram of this parameter R_i is shown in Figure 4 together with the expectation for a Gaussian distribution of parallaxes. It can be clearly seen that the data is in good agreement with a Gaussian distribution. Hence, the fitting results are dominated by statistical and not by systematic errors.

An annual parallax for W3(OH) of 0.484 ± 0.004 kpc corresponds to a distance of $2.07^{+0.01}_{-0.02}$ kpc. Georgelin & Georgelin (1976) estimated a kinematic distance of 2.3 kpc for W3(OH) and Humphreys (1978) estimated a photometric distance of 2.2 kpc to the OB association near W3(OH).

4. Conclusion

We estimated an annual parallax of 0.484 ± 0.004 mas for W3(OH) from the absolute proper motions of associated H₂O maser features. This corresponds to a distance of $2.07^{+0.01}_{-0.02}$ kpc and is consistent with past determinations.

The absolute proper motion is the sum of the annual parallax and a linear component. The linear component includes the inner motion of each maser feature, which can be estimated independently from the motion relative to a reference maser feature. After subtracting the inner motions, all maser components will have the same proper motions. The linear part of these motions can be determined from maser features which are detected in more than five epochs. Thus, we can decrease the number of free parameters by fixing the linear component. Then we can also use components which are detectable in less than 5 epochs. This has the potential to increase the accuracy of the annual parallax even further. We will also get the total proper motion of W3(OH) from this observation and this will help to constrain models of the Galactic rotation. This will be the subject of an upcoming paper.

There are other H₂O of other maser sources with close-by positional reference sources in the Galaxy. Thus, it is possible to determine the distance of other maser sources with phase-referencing VLBI astrometric observations with similar accuracy to the case of the H₂O masers in W3(OH). We are planning an extensive program to use parallax and proper motion measurements to constrain Galactic structure and rotation.

Acknowledgements. We are grateful to Dr. Mark Reid for very helpful discussions.

References

- Alcolea, J., Menten, K. M., Moran, J. M., & Reid, M. J. 1992, in *Astrophysical Masers*, ed. A. W. Clegg & G. E. Nedoluha (Heidelberg:Springer), 225
- Beasley, A. J., & Conway, J. E. 1995, *Very Long Baseline Interferometry and the VLBA*, ed. J. A. Zensus, P. J. Diamond, & P. J. Napier (San Francisco: ASP), ASP Conf. Ser., 82, 328
- Briskin, W. F., Benson, J. M. & Goss, W. M., 2002, *Ape*, 571, 906
- Brunthaler, A., Reid, M. J. & Falcke, H., 2003, *astro-ph/0309575*
- Fey, A. L. & Charlot, P. 2000, *ApJS*, 128, 17
- Georgelin, Y. M., & Georgelin, Y. P. 1976, *A&A*, 49, 57
- Margon, B. & Kwitter, K. B. 1978, *Apj*, 224, L43
- Perryman, M. A. C., Lindegren, L., Kovalevsky, J., et al. 1995, *A&A*, 304, 69
- Reid, M. J., Argon, A. L., Masson, C. R., et al. 1995, *ApJ*, 238, 443
- Ros, E. 2003, *astro-ph/0308265*
- van Langevelde, H. J., Vlemmings, W., Diamond, P. J., et al. 2000, *A&A*, 357, 945
- Vlemmings, W., van Langevelde, H. J., Diamond, P. J., et al. 2003, *A&A*, 407, 213
- Wouterloot, J.G.A., Brand, J., & Fiegle, K. 1993, *A&AS*, 98, 589
- Wyrowski, F., Schilke, P., Walmsley, C. M., & Menten, K. M. 1999, *ApJ*, 514, L43